A COMPARISON OF STATISTICAL SEGMENTATION TECHNIQUES FOR POLARIMETRIC SAR: REGION GROWING VERSUS SIMULATED ANNEALING

T. Macrì Pellizzeri[(1)], P. Lombardo[(1)], C. J. Oliver[(2)], M. Sciotti[(1)], M. Meloni[(1)], I. McConnell[(2)]

[(1)] University of Rome "La Sapienza" – Via Eudossiana 18 - 00184 Rome, Italy.
Ph. +39-0644585412 Fax: +39-064873300 E-mail: t.macri.pellizzeri@infocom.uniroma1.it
[(2)] InfoSAR Ltd., Roscoe House, 62 Roscoe ST., Liverpool L1 9DW, UK.
Ph: +44 (0)151 7095065; Fax: +44 (0)151 7095645; e-mail chris@infosar.co.uk

ABSTRACT

In this paper, two polarimetric segmentation techniques for polarimetric SAR images are compared. They are both based on the maximum generalised likelihood approach and on a Wishart distribution model. The first technique, named POLSEGANN, is based on a global likelihood approach and on the simulated annealing maximization technique, while the second one (POL MUM) is based on a Maximum Likelihood (ML) Split-Merge test between adjacent regions, and on a region growing scheme. Both techniques exploit the properties of the covariance matrix of the data, but they proceed with very different approaches to identify the widest possible homogeneous segments. The comparison of the two techniques is performed both on a wide set of simulated images and on real data. Results are evaluated qualitatively and quantitatively, considering the accuracy achieved in the classification of the segmented images and the statistical characteristics of the ratio image. We show that POLSEGANN provides more accurate classification results and a better identification of small regions, while POL MUM provides an accurate statistical reconstruction of the original image, and the identification of large homogeneous regions.

1. INTRODUCTION

The extraction of information from polarimetric SAR images, that carry appreciably more information about the observed scene than the single-channel SAR images, is still an area of active research for the many operational polarimetric SAR sensors that are becoming available in the very near future. In particular, an interesting approach to the extraction of information consists in applying segmentation to the SAR images before any further operation (classification, feature extraction, etc..). In fact, it has been clearly demonstrated ([1], [11]) that large performance improvement can be achieved by first segmenting the SAR image into homogeneous regions, and then classifying the resulting regions. It is therefore of interest to define optimal segmentation techniques for the polarimetric SAR images. Many previous works were related more with the exploitation of both the reflectivity and the phase relationship between the different polarimetric channels to extract useful indications on the characteristics of the different observed objects, allowing a more accurate classification [1-4]. Many examples of terrain classification using polarimetric data can be easily found in literature, with application to very different monitoring and surveillance tasks [5-10]. The theory at the basis of effective approaches for segmentation of polarimetric SAR images has been proposed by the authors in [12], [13]. These works presented the derivation of the generalised likelihood function of a single segment of polarimetric SAR image. This was shown to be the basic step to obtain both the global generalised likelihood of the whole image and the Split-Merge test between two adjacent regions. Then, the global generalised likelihood was used in connection with a simulated annealing approach to derive a polarimetric segmentation scheme, named POLSEGANN. In this paper, we introduce a region growing technique (POL MUM) for segmenting the polarimetric SAR images, based on the optimal Split-Merge test. The resulting algorithm is then compared to POLSEGANN to assess their comparative theoretical performance both on a wide set of simulated data and on real data. A full set of cases is studied to generate a complete simulated comparison of the techniques. We consider three different sets of images, each one characterised by different statistical properties for the regions, with the aim of better assessing the performance of the two techniques in different operating conditions. Finally, the two techniques are applied to an ESAR image of agricultural land, to compare their behaviour on real data. The paper is organized as follows. In Section 2 we define the adopted statistical model and provide a short description of the derivation of the POLSEGANN technique. The derivation of the POL MUM segmentation technique is illustrated in Section 3, while Section 4 describes the generation of the simulated dataset. The comparison of the results achieved with the different techniques for all the considered cases is reported in Section 5, while the application to real data is discussed in Section 6. Finally, our conclusions are drawn in Section 7.

2. DATA MODEL

Let us assume that we operate on fully calibrated polarimetric SAR images, in order to focus on the polarimetric signal processing techniques only. Consider a single region and arrange the echoes received from the same resolution cell on the M polarimetric channels into the vector $\mathbf{x} = [x_1, \cdots, x_M]^T$ (where for example $x_1=x_{HH}$, $x_2=x_{VV}$, $x_3=x_{HV}$). Assuming the

absence of texture, the joint Probability Density Function (PDF) of the N pixels of a single region can be written as

$$p(\mathbf{x}) = \pi^{-MN} |R|^{-N} exp\left[- Tr\left\{\mathbf{R}^{-1}\sum_{n=1}^{N}\mathbf{x}_n\mathbf{x}_n^H\right\}\right] \quad (1)$$

where **R** is the polarimetric complex covariance matrix and Tr{**A**}and |**A**| stand for the trace and the determinant of the matrix **A** respectively. Eq. (1) also defines the likelihood of the N pixels belonging to a region with known covariance matrix **R**. Since in general **R** is not known a priori, the likelihood function cannot be used directly. Therefore, we resort to the generalised likelihood, by replacing the unknown covariance matrix with its Maximum Likelihood (ML) estimate. It is easily shown that the estimated polarimetric covariance matrix is given by the sample covariance matrix estimated on the N-pixel region, so that the generalised likelihood function L(x) of a homogeneous region of N pixels is

$$L(\mathbf{x}) = Max_R\{p(\mathbf{x})\} = \left(\frac{N}{\pi e}\right)^{MN}\left|\sum_{n=1}^{N}\mathbf{x}_n\mathbf{x}_n^H\right|^{-N} \Rightarrow \quad ln[L(\mathbf{x})] = Max_R\{p(\mathbf{x})\} = MN\,ln\left(\frac{N}{\pi e}\right) - N\,ln\left(\left|\sum_{n=1}^{N}\mathbf{x}_n\mathbf{x}_n^H\right|\right) \quad (2)$$

Based on eq. (2), we can write the Joint Logarithmic Likelihood (JLL) of the whole image, which is assumed to be composed of Q regions with $N_1,\ldots,N_Q$ pixels. Assuming the pixel intensities spatially independent, the JLL is given by:

$$\Lambda_{POLSEGANN} = \sum_{q=1}^{Q} MN_q\left[ln(N_q) - ln(\pi e)\right] - \sum_{q=1}^{Q} N_q\,ln\left(\left|\sum_{n=1}^{N_q} x_n^{(q)}x_n^{(q)H}\right|\right) = -MN\,ln(\pi e) - \sum_{q=1}^{Q} N_q\,ln\left(N_q^{-1}\left|\sum_{n=1}^{N_q} x_n^{(q)}x_n^{(q)H}\right|\right) \quad (3)$$

To derive a ML polarimetric segmentation technique, eq. (3) can be used in connection with a maximization technique, such as the simulated annealing, as the objective function to be maximized. The corresponding grouping of pixels in the Q regions gives the optimum segmentation of the polarimetric SAR image, according to the generalized likelihood criterion. The resulting polarimetric segmentation technique (POLSEGANN) makes full use of the polarimetric characteristics of the back-scattering from the observed scene, and is expected to yield the full geometrical resolution, by working directly on the original data, while exploiting the full polarimetric covariance matrix to increase the discrimination capability. To avoid the presence of segments with non-smooth borders, a curvature penalty function is added to the function in eq. (3) to form the objective function of the annealing procedure. The penalty function is controlled by a shape parameter *s*, that can be set by the user.

3. MERGE USING MOMENTS SEGMENTATION TECHNIQUE

Following the maximum likelihood approach, a ML Split-Merge test can be derived. This is based on the generalised likelihood function in eq. (2), and is required to test whether two regions A and B, with N_A and N_B pixels respectively, belong to the same statistic (and thus must be merged): hypothesis H_0, or do not belong to the same statistic (and thus must be split): hypothesis H_1. The generalised likelihood ratio test for the two hypotheses yields

$$\Lambda_M = \frac{max_{\mathbf{R}^{(0)}}\left\{p_{\mathbf{x}^{(A)},\mathbf{x}^{(B)}}(\mathbf{x}^{(A)},\mathbf{x}^{(B)}/\mathbf{R}^{(0)})\right\}}{max_{\mathbf{R}^{(A)}}\left\{p_{\mathbf{x}^{(A)}}(\mathbf{x}^{(A)}/\mathbf{R}^{(A)})\right\}\cdot max_{\mathbf{R}^{(B)}}\left\{p_{\mathbf{x}^{(B)}}(\mathbf{x}^{(B)}/\mathbf{R}^{(B)})\right\}} = C^{M}\cdot\frac{\left|\sum_{n=1}^{N_A}\mathbf{x}_n^{(A)}\mathbf{x}_n^{(A)H}\right|^{N_A}\left|\sum_{n=1}^{N_B}\mathbf{x}_n^{(B)}\mathbf{x}_n^{(B)H}\right|^{N_B}}{\left|\sum_{n=1}^{N_A}\mathbf{x}_n^{(A)}\mathbf{x}_n^{(A)H}+\sum_{n=1}^{N_B}\mathbf{x}_n^{(B)}\mathbf{x}_n^{(B)H}\right|^{N}} > \lambda \quad (4)$$

where $\mathbf{R}^{(A)}$ and $\mathbf{R}^{(B)}$ are the covariance matrices of the two different regions in hypothesis H_1, $\mathbf{R}^{(0)}$ is the common covariance matrix in the hypothesis H_0, the constant C is given by $C = N^N/(N_A^{N_A}N_B^{N_B})$, and λ is an appropriate threshold. The Split-Merge test in eq. (4) is the basic step of the proposed region-growing segmentation technique. The split-merge approach, named Polarimetric Merge-Using-Moments (POL MUM), has presently been implemented into an effective segmentation routine. Specifically, POL MUM iteratively tests adjacent segments for homogeneity and merges the most homogeneous set of adjacent segments. Only segments with differences higher than a pre-assigned value can be merged, which yields a stop criterion to the algorithm. For this purpose, the value of the test threshold is related to the probability of erroneously deciding to split segments with the same polarimetric properties, named the probability of false alarm (P_{fa}). Therefore, an analytic expression is required for the P_{fa} as a function of the number of pixels in the regions under test. Unfortunately, the PDF of the generalized likelihood ratio under the Merge hypothesis is not known, thus the exact expression of P_{fa} is not available Consequently, we resort to an approximate expression,

$$P_{fa} = \gamma\left(M^2/2, -\rho\,ln\,\lambda\right) + \beta\left[\gamma\left(M^2/2+2, -\rho\,ln\,\lambda\right) - \gamma\left(M^2/2, -\rho\,ln\,\lambda\right)\right] + O\left(\rho^3 N^3\right), \quad (5)$$

$$\rho = 1 - \frac{M^2-1}{6M}\left(\frac{1}{N_A}+\frac{1}{N_B}-\frac{1}{N}\right) \qquad \beta = \frac{M^2}{12\rho^2}\left[\frac{M^2-1}{2}\left(\frac{1}{N_A^2}+\frac{1}{N_B^2}-\frac{1}{N^2}\right) - 3(1-\rho)^2\right]. \quad (6)$$

where $\gamma(v,x)$ is the incomplete Gamma function of order *v* and argument *x*, and ρ and β are defined as in eq. (6).

4. GENERATION AND CHARACTERISTICS OF THE SIMULATED DATASET

To compare the performance of the segmentation techniques described in Sec. 2 (POLSEGANN) and in Sec. 3 (POL MUM), we consider a wide set of synthetic 3-channel complex images. All the images are obtained from the same pattern of regions, composed of 25 distinct segments belonging to seven different classes, each one characterized by a different covariance matrix. The pattern is shown in Fig.1a, where each class corresponds to a different colour. The correspondence between classes and colours is the following: class 1 – dark blue, class 2 – blue, class 3 – light blue, class 4 – green, class 5 – yellow, class 6 – orange, class 7 - red. We consider three different sets of covariance matrices for the seven classes, each set characterised by different properties. In the first case (A), the covariance matrices of all the seven classes have the same determinant, while the average intensity of the three channels is different for different classes. Moreover, in this case the average intensity of one of the channels is approximately one tenth of the average intensities of the other two channels. This is intended to be representative of many practical applications, where the average power of the cross-polarized channel is significantly smaller than the power of the co-polarized channels. In the second case (B), all the covariance matrices have the same trace, namely the sum of the average intensities of the three channels is the same for all the classes. Moreover, the average intensity of the second channel is definitely higher than the other two. Finally, in the third case (C) there is not a common characteristic for the covariance matrices of all the classes, but only for some of them. More in detail, in this case some classes have the same determinant of the covariance matrix, and others show very similar values for the trace. Following the model in eq. (1), for each case we generate a set of 10 random independent single-look images with the same statistical characteristics in a MonteCarlo simulation. As an example, the intensities of channels 1 and 2 of the first trial in case B are reported in Fig. 1b and 1c respectively. Then both POLSEGANN and POL MUM are fed with the same data, considering different values of the curvature parameter s in the first case, and different values of P_{fa} in the second. In both cases, we select the value maximizing the probability of correct classification against the test pattern, averaged over the set of simulations. To provide a quantitative measure of the quality of the different segmentation schemes, we apply the same classifier to the identified regions. In particular, we use a ML supervised classifier, based on the statistical model in eq. (1), assuming that the polarimetric characteristics of the seven classes c = 1, …, 7 are known (i.e. their covariance matrix $\mathbf{R_c}$ is known). Thus, the generic segment of N pixels is assigned to class $\hat{c}$ that minimises the corresponding likelihood:

$$\hat{c} = arg\ min_c \left\{ ln\left(\left|\mathbf{R}_c\right|\right) + Tr\left[\mathbf{R}_c^{-1} \frac{1}{N} \sum_{n=1}^{N} \mathbf{x}_n \mathbf{x}_n^H \right] \right\} = arg\ min_c \left\{ ln\left(\left|\mathbf{R}_c\right|\right) + Tr\left[\mathbf{R}_c^{-1} \hat{\mathbf{R}}\right] \right\} \quad (7)$$

where $\hat{\mathbf{R}}$ is the sample covariance matrix estimated on the whole segment.

5. COMPARATIVE ANALYSIS OF THE RESULTS

To compare the achieved segmentation results we apply the ML classification scheme in eq. (7) to the identified segments, and evaluate the average confusion matrix and the average probability of correct classification. The confusion matrix reports on each row the percentage of pixels belonging to a given class that have been assigned to all the possible classes, while the probability of correct classification, P_{cor}, is the average of the percentages of correctly classified pixels for each class. Their average values are reported in Tabs.1, 2, and 3 for the three cases, while the best classifications are shown in Fig. 2a-c for POLSEGANN, and in Fig. 3a-c for POL MUM. Classification results allow us to discuss the ability of the proposed techniques to discriminate between adjacent regions belonging to different classes with similar properties. Moreover, the value of P_{cor} yields a global measure of segmentation correctness, since a bad segmentation implies a bad classification. From the comparison of the achieved results, it is apparent that POLSEGANN performs better than POL MUM in cases A and C, while performance is the same for case B. The difference between the results achieved with the two methods is mainly due to the poor performance of POL MUM in the identification of class 3. This class is composed of a reduced number of pixels, thus a small error in the identification of its borders leads to a significant performance degradation. As apparent from Figs. 2a-c and 3a-c, in the classifications obtained with POLSEGANN this class has a more regular shape than in the POL MUM case. On the contrary, it is apparent that in case B the POL MUM algorithm performs better than POLSEGANN in the identification of the borders, especially for the straight ones, and the same can be noticed also in the other cases. This is probably due to intrinsic characteristics of the two algorithms (the initial tessellation of the images in the POL MUM algorithm helps the formation of straight borders), and also to a different penalty in case of non-smooth borders. As a final remark, the global annealing method might be expected to provide a slightly better classification than the local MUM technique, as is indeed indicated in the confusion matrices. However, the distinction is likely to be more marked when a more realistic test pattern is adopted, with smaller regions. It must be noted that the comparison of the proposed techniques in terms of classification accuracy is not the only possible criterion. It was adopted here since an unambiguous comparison of classification performance could be defined and is related to a real remote sensing problem. Another set of criteria would be associated with attempting to quantify the segmentation quality. A variety of statistical tests can be applied to

determine whether the ratio image of the original intensity to its segmentation satisfies the speckle model [15]. A different criterion would be to assert that "good" segmentation. should grow large regions. To determine how the two algorithms compare on the basis of these criteria it would be necessary to optimise the shape parameter in simulated annealing and the false alarm parameter in MUM against the different measures. It would be hoped that a good algorithm would not show dramatic variations in the value of the parameters used to optimise the different measures.

Original class \ Assigned class	1	2	3	4	5	6	7
1	97.1	0.3	0.0	0.5	0.5	0.6	0.9
2	2.9	88.5	0.1	0.7	1.9	0.2	5.5
3	1.2	0.0	51.3	5.9	18.1	22.4	1.2
4	0.3	0.7	1.6	90.0	0.1	0.4	7.0
5	1.8	0.4	0.3	0.0	96.5	0.6	0.4
6	0.8	0.3	0.7	0.2	0.3	96.7	0.9
7	3.1	2.2	0.1	1.5	0.1	1.1	91.9

(a)

Original class \ Assigned class	1	2	3	4	5	6	7
1	96.0	0.6	0.1	0.3	0.5	0.3	2.3
2	3.1	80.7	0.1	1.2	1.6	0.7	12.8
3	1.9	0.0	44.1	2.3	16.3	35.3	0.2
4	0.3	0.7	0.3	90.3	0.0	0.2	8.2
5	2.9	0.2	0.6	0.4	94.5	0.7	0.8
6	0.9	0.3	1.3	0.8	0.4	95.1	1.3
7	3.7	1.0	0.1	4.0	0.2	0.8	90.2

(b)

Pcor	
POL SEGANN	87.4 ±4.0
POL MUM	84.4± 3.1

Tab. 1 – average confusion matrices for case A. (a) POLSEGANN; (b) POL MUM

Original class \ Assigned class	1	2	3	4	5	6	7
1	98.2	0.1	0.1	0.3	0.3	0.2	0.8
2	0.1	99.6	0.0	0.0	0.1	0.0	0.2
3	1.2	0.0	77.9	0.5	14.8	5.6	0.0
4	0.3	0.1	0.4	95.8	0.1	0.1	3.3
5	1.5	0.2	0.3	0.0	97.3	0.4	0.2
6	0.6	0.1	0.1	0.0	0.2	98.2	0.7
7	0.4	0.2	0.0	0.4	0.0	0.2	98.8

(a)

Original class \ Assigned class	1	2	3	4	5	6	7
1	99.3	0.0	0.0	0.1	0.2	0.1	0.2
2	0.1	99.3	0.1	0.0	0.0	0.1	0.4
3	2.3	0.0	78.1	0.0	12.5	6.9	0.3
4	0.0	0.0	0.1	98.2	0.0	0.0	1.7
5	1.7	0.0	0.9	0.1	96.7	0.5	0.1
6	0.2	0.0	0.1	0.0	0.3	99.4	0.1
7	0.6	0.0	0.0	1.3	0.0	0.1	98.0

(b)

Pcor	
POL SEGANN	95.1 ±0.5
POL MUM	95.6 ± 0.7

Tab. 2 – average confusion matrices for case B. (a) POLSEGANN; (b) POL MUM

Original class \ Assigned class	1	2	3	4	5	6	7
1	97.7	0.4	0.0	0.2	0.4	0.4	0.8
2	1.0	97.2	0.0	0.2	0.8	0.2	0.6
3	1.1	0.0	68.3	4.2	16.8	9.4	0.2
4	0.2	0.4	0.7	92.2	0.0	0.1	6.3
5	1.6	0.5	0.4	0.0	96.9	0.5	0.1
6	1.1	0.2	0.5	0.2	0.3	96.6	1.2
7	2.4	0.5	0.1	1.5	0.1	0.8	94.6

(a)

Original class \ Assigned class	1	2	3	4	5	6	7
1	95.4	0.4	0.3	0.9	0.5	0.2	2.4
2	1.7	92.8	0.2	0.4	1.1	0.5	3.3
3	1.1	0.7	54.8	2.4	14.8	25.6	0.6
4	1.5	0.5	1.4	88.0	0.4	0.3	7.9
5	1.8	1.1	0.7	0.2	94.8	0.9	0.6
6	0.4	0.7	1.4	0.3	0.6	95.5	1.2
7	3.4	1.2	0.4	3.3	0.5	0.9	90.4

(b)

Pcor	
POL SEGANN	91.9 ±1.9
POL MUM	87.4 ±2.4

Tab. 3 – average confusion matrices for case A. (a) POLSEGANN; (b) POL MUM

It must also be appreciated that the local merge criterion involved in MUM separates pairs of regions whose properties differ by some defined amount. The global annealing algorithm applies a global error analysis to determine whether pixels should change from one region to another. In fact, annealing is often followed by a merge stage to remove boundaries between neighbouring regions which are statistically insignificant. This has an appreciable effect on the statistics of the residual ratio and, in particular, its PDF. In practice, both algorithms can be tuned to yield statistical results arbitrarily close to theory.

	Average N	Average CV	Std CV	Average NL	Std NL
Theoretical results	25	0.999258	0.007801	-0.577023	0.003137
POLSEGANN case A	146.4	0.990415	0.006834	-0.57402	0.002862
POL MUM case A	111.5	0.996835	0.007106	-0.57642	0.003124
POLSEGANN case B	127	0.994413	0.007302	-0.57456	0.003617
POL MUM case B	39.6	1.002156	0.00726	-0.57758	0.003553
POLSEGANN case C	136.2	0.991711	0.008696	-0.57414	0.003378
POL MUM case C	124.1	0.997664	0.010304	-0.57654	0.003624

Tab. 4 – Average and Standard deviation of the estimated CV and NL.

We remove real structure from the scene to compensate for speckle noise which has not been removed. Tab. 4 compares a variety of measures, suggested by [15], applied to the segmentations optimised for classification accuracy. The average number of segments (N) is always significantly greater than the known value, with POLSEGANN generally finding more segments than POL MUM. This is particularly apparent for case B. It should be noted that comparatively small changes in the shape parameter can modify region size significantly without degrading classification accuracy much. This means that the optimum position lies in a rather broad range of parameter values. The average and the standard deviation of both the

variance of the intensity ratio image (Coefficient of Variation, CV) and the average logarithmic intensity of the ratio image (Normalised Log, NL) in Table 4 also indicate that POL MUM is closer to theoretical prediction. A large part of the difference is probably due to the smaller segment size so that changing that, by varying the shape parameter, would have an appreciable effect on those measures. What is required is a more detailed comparative study of the algorithms against other quality measures. Generally speaking, the regions will be much smaller and will not have structures aligned to image axes. A complete supervised classification process will be simulated as one form of comparison. We shall also address some of the issues of segmentation quality and attempt to show the importance of segmentation quality, as a pre-processing stage, in more realistic land studies.

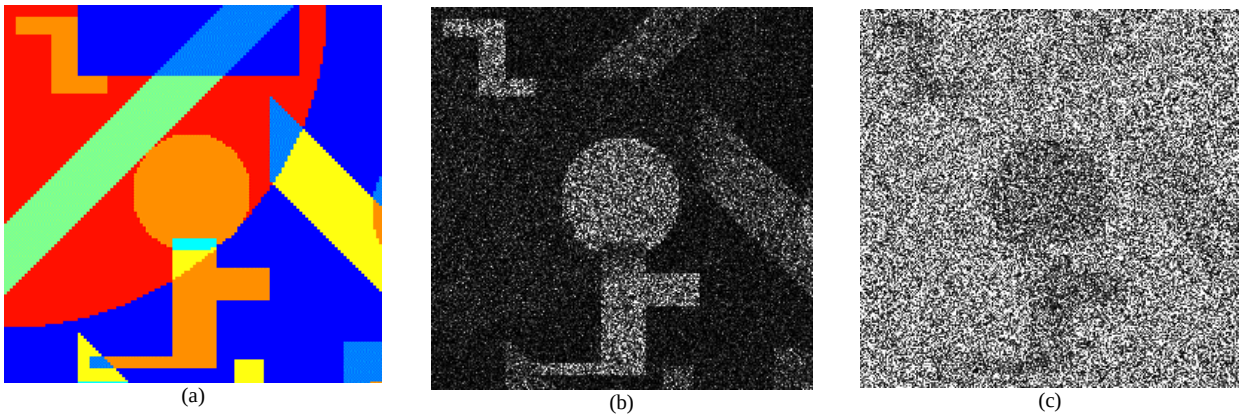

(a) (b) (c)

Fig. 1 Simulated dataset. Original pattern of regions (a), intensity image for the first trial of case B: channel 1 (b), and channel 2 (c).

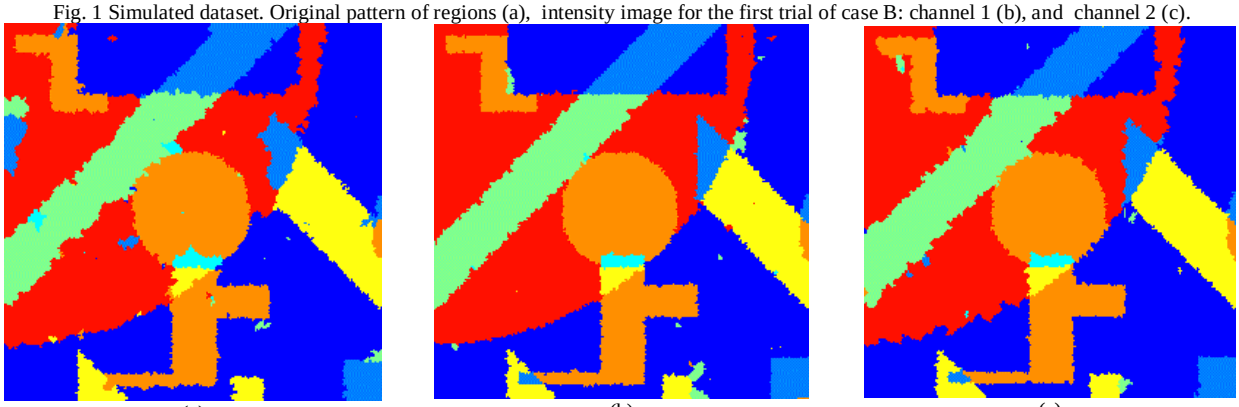

(a) (b) (c)

Fig. 2 – Best classification with POLSEGANN for a) case A, b) case B, and c) case C.

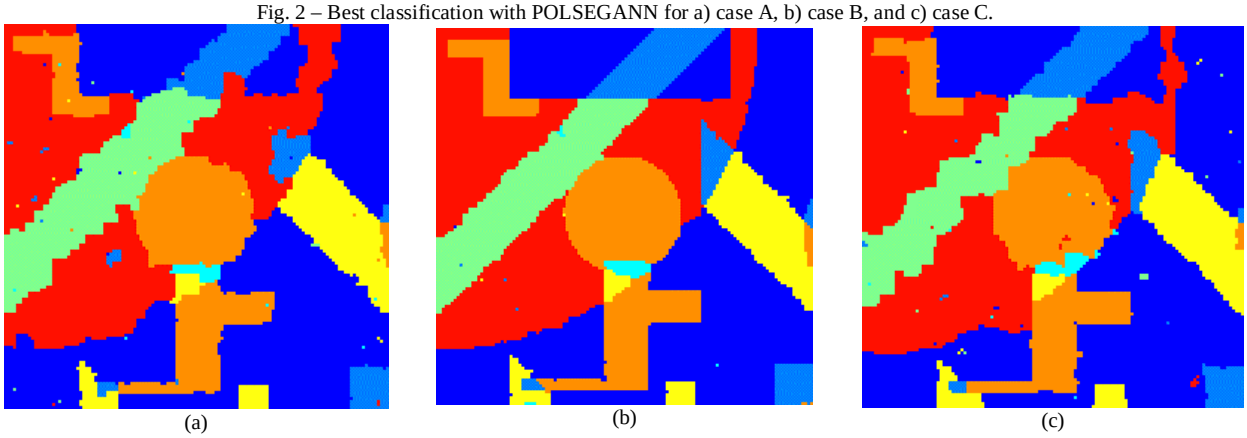

(a) (b) (c)

Fig. 3 – Best classification with POL MUM for a) case A, b) case B, and c) case C.

6. APPLICATION TO REAL DATA

To provide a first assessment of the comparative performance of the two techniques on real data, they are applied to an ESAR image of an agricultural area near Oberpfaffenhoffen, in Germany. The corresponding segmented images are shown in Figs. 5 and 6 for POLSEGANN and POL MUM respectively. As apparent, the application to real images tends to confirm the results obtained on simulated data. In particular, it can be easily noted that POL MUM identifies a

smaller number of segments than POLSEGANN, but the initial tessellation degrades the definition of region borders, especially when they are not aligned with it. On the contrary, POLSEGANN allows a better identification of region borders, together with a more accurate identification of the small details.

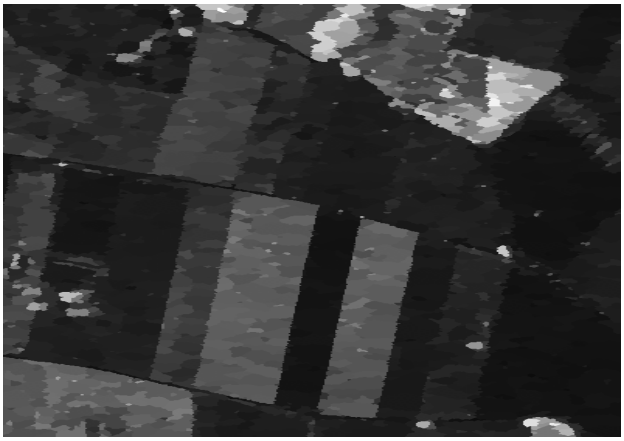

Fig. 5 – Segmentation of the ESAR image with POLSEGANN

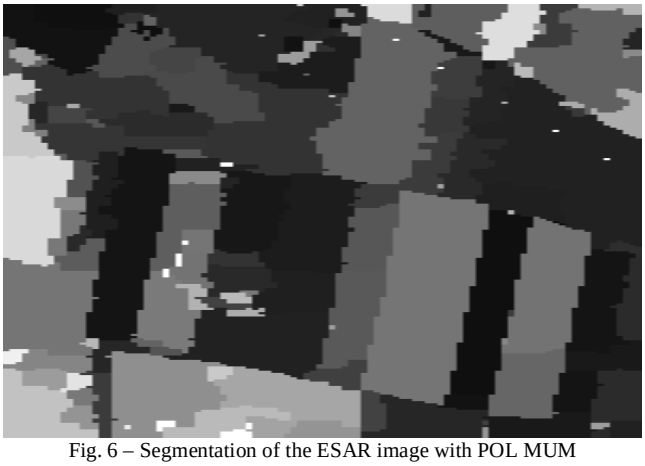

Fig. 6 – Segmentation of the ESAR image with POL MUM

7. CONCLUSIONS

In this work we compared two different segmentation algorithms for polarimetric SAR images, both based on a generalised likelihood approach. The POLSEGANN algorithms is based on a maximisation of the global likelihood of the image through simulated annealing, while the POL MUM algorithm is based on a region growing scheme and a ML Split-Merge test. They were applied on a wide set of simulated images, and the results were compared both in terms of classification accuracy and statistical characteristics of the ratio image. The achieved results show that POLSEGANN performs better when considering the classification of the achieved segments. This is especially true for small regions, that tend to be confused with the adjacent ones by the POL MUM algorithm. On the contrary, large regions are more accurately identified with the POL MUM algorithm, that also tends to provide a more accurate statistical reconstruction of the original pattern of regions.

8. REFERENCES

1. Oliver, C.J. and Quegan, S., *Understanding SAR images*, Artech House, New York, U.S.A., 1998.

2. Van Zyl J.J., Zebker H.A. and Elachi C., Imaging radar polarization signatures: Theory and observations, *Radio Science*, Vol. 22, 529 - 543, 1987.

3. Ulaby F.T. and Elachi, C., *Radar Polarimetry for Geoscience Applications*, Artech House, Norwood, 1990.

4. Zebker H.A. and Van Zyl J.J., Imaging radar polarimetry: A review, *IEEE Proceedings*, Vol. 79, 1583 - 1606, 1991.

5. Novak L. M. and Burl M. C., Optimal speckle reduction in polarimetric SAR imagery, *IEEE Trans. on Aerospace Electronic Systems*, Vol. 26, 293 - 305, 1990.

6. Lee J., Grunes, M. R. and Mango, S. A., Speckle reduction in multipolarisation, multifrequency SAR imagery, *IEEE Trans. on Geoscience and Remote Sensing*, Vol. 29, 535 - 544, 1991.

7. Lombardo P. and Oliver C.J., Optimum Detection and Segmentation of oil-slicks using polarimetric SAR data, *IEE Proceedings on Radar, Sonar and Navigation*, Vol. 147, No. 6, 2000.

8. Cloude S.R. and Pottier E., A Review of Target Decomposition Theorems in Radar Polarimetry, *IEEE Trans. on Geoscience and Remote Sensing*, Vol. 34, 498 - 518, 1996.

9. Cloude S. R. and Pottier E., An entropy based classification scheme for land applications of polarimetric SAR, *IEEE Trans. on Geoscience and Remote Sensing*, Vol. 35, 68 - 78, 1997.

10. Lee J.-S. and Hoppel K. W., Principal components transformation of multifrequency polarimetric SAR imagery, *IEEE Trans. on Geoscience and Remote Sensing*, Vol. 30, 686 - 696, 1992.

11. Macrì Pellizzeri T., Oliver C.J. and Lombardo P., Segmentation-Based Joint Classification of SAR and Optical Images, *IEE Proceedings on Radar Sonar and Navigation*, Vol. 149, 281-296, 2002.

12. Lombardo P., Oliver C.J., Optimal Classification of Polarimetric SAR images Using Segmentation, *IEEE Radar Conference 2002*, Long Beach (CA), April 2002.

13. Lombardo P., Oliver C.J., Optimal Polarimetric Segmentation for the Classification of Agricultural Areas, *EUSAR 2002*, Koeln, Germany, June 2002.

14. Abramowitz M. and Stegun I.A., *Handbook of mathematical functions*, Dover Publications, New York, U.S.A., 1970.

15. Caves R., Quegan S., and White R., Quantitative comparison of the Performance of SAR Segmentation Algorithms, *IEEE Trans. on Image Processing*, Vol. 7, 1534-1546, 1998.